PHYSICAL REVIEW APPLIED **2,** 024006 (2014)

Composition-Structure-Property Relations of Compressed Borosilicate Glasses

Mouritz N. Svenson,[1] Tobias K. Bechgaard,[1] Søren D. Fuglsang,[1] Rune H. Pedersen,[1] Anders Ø. Tjell,[1]
Martin B. Østergaard,[1] Randall E. Youngman,[2] John C. Mauro,[2] Sylwester J. Rzoska,[3,4]
Michal Bockowski,[3] and Morten M. Smedskjaer[1,*]
[1]*Section of Chemistry, Aalborg University, 9000 Aalborg, Denmark*
[2]*Science and Technology Division, Corning Incorporated, Corning, New York 14831, USA*
[3]*Institute of High Pressure Physics, Polish Academy of Sciences, 01-142 Warsaw, Poland*
[4]*Institute of Physics, University of Silesia, 41-500 Chorzow, Poland*
(Received 7 April 2014; revised manuscript received 11 June 2014; published 14 August 2014)

Hot isostatic compression is an interesting method for modifying the structure and properties of bulk inorganic glasses. However, the structural and topological origins of the pressure-induced changes in macroscopic properties are not yet well understood. In this study, we report on the pressure and composition dependences of density and micromechanical properties (hardness, crack resistance, and brittleness) of five soda-lime borosilicate glasses with constant modifier content, covering the extremes from Na-Ca borate to Na-Ca silicate end members. Compression experiments are performed at pressures ≤1.0 GPa at the glass transition temperature in order to allow processing of large samples with relevance for industrial applications. In line with previous reports, we find an increasing fraction of tetrahedral boron, density, and hardness but a decreasing crack resistance and brittleness upon isostatic compression. Interestingly, a strong linear correlation between plastic (irreversible) compressibility and initial trigonal boron content is demonstrated, as the trigonal boron units are the ones most disposed for structural and topological rearrangements upon network compaction. A linear correlation is also found between plastic compressibility and the relative change in hardness with pressure, which could indicate that the overall network densification is responsible for the increase in hardness. Finally, we find that the micromechanical properties exhibit significantly different composition dependences before and after pressurization. The findings have important implications for tailoring microscopic and macroscopic structures of glassy materials and thus their properties through the hot isostatic compression method.

DOI: 10.1103/PhysRevApplied.2.024006

I. INTRODUCTION

Crystalline materials of the same chemical composition can undergo first-order phase transformations at high pressure into polymorphs with unusual chemical and physical properties due to different short- and long-range ordering and symmetries. Compression is thus an important tool in the synthesis of novel crystalline materials, as demonstrated, e.g., by the high-pressure synthesis of new superconductors [1]. While the effects of pressure on the structure and various macroscopic properties of glasses (e.g., density and viscosity) have been extensively studied [2], comparable breakthroughs in using compression as a method to prepare bulk silicate glassy materials with novel performances on an industrial scale are still largely lacking. This gap exists despite the fact that glasses can also undergo an analogous phenomenon known as polyamorphism [3,4]. Polyamorphism is observed in different glass compositions, such as the low-density and high-density glassy phases of water [5–8]. While such polyamorphic phases may exhibit interesting properties, they usually form at very high pressures and/or temperatures. These conditions currently inhibit the preparation of samples of large geometry, traditionally not reaching above 1 GPa for samples of 20 mm maximum diameter. Furthermore, and to the best of our knowledge, so far no definitive evidence for polyamorphism in silicate glasses, which are the most important materials for the glass industry [9], has been reported.

However, besides the first-order polyamorphic transitions, glasses can exhibit continuous changes in short- and intermediate-range order during pressurization. Consequently, it is possible to tune the atomic bonding and packing density of bulk glass samples and thereby alter their macroscopic physical properties. Such compression usually has to be done at elevated temperature (e.g., around the glass transition temperature T_g), since most structural changes at room temperature are reversible upon decompression at pressures below 5–10 GPa [10,11]. Isostatic compression of bulk oxide glasses at pressures up to 1 GPa around T_g is found to increase density, refractive index, elastic moduli, and hardness, whereas crack resistance and fracture toughness decrease [12–18]. In order to

---

[*]Corresponding author.
mos@bio.aau.dk

© 2014 American Physical Society

design new glass compositions with novel property combinations through quenching from the high-pressure–high-temperature condition, detailed understanding of the structural and topological origins of these changes and their compositional dependences is required. Tuning the mechanical properties of glasses is especially important given the increasing demand for stronger, thinner, and more flexible glasses in recent years [19–21].

In this work, we investigate the effect of chemical composition on the pressure-induced changes in density and micromechanical properties of bulk borosilicate glasses. Specifically, we investigate the effects of B_2O_3-for-SiO_2 substitutions in soda-lime borosilicate glasses with fixed modifier content, covering the extremes from Na-Ca borate to Na-Ca silicate end members. The system is interesting, since different structural and topological rearrangements are found to occur upon compression, such as an increase of the average coordination number of B^3, while that of Si^{4+} is unaffected within this pressure-temperature regime [15]. Moreover, this series contains abundant topological and structural features, e.g., the variation of boron speciation with chemical composition. The present study sheds light on the structural units responsible for the pressure-induced changes in macroscopic properties, which is further investigated through supplementary nuclear-magnetic-resonance (NMR) measurements. For example, we demonstrate a strong correlation between the plastic compressibility and the initial trigonal boron content in the soda-lime borosilicate glasses. This compressibility feature of the trigonally coordinated boron atoms has been directly applied in the design of a recent commercial glass (Corning® Gorilla® Glass 3) [22].

II. EXPERIMENTAL

Glasses in the system $(75-x)SiO_2$-xB_2O_3-$15Na_2O$-$10CaO$, with $x = 0$, 15, 37, 50, and 75 were investigated. The three glasses with $x = 37$, 50, and 75 were taken from previous studies [17,23]. All of the glasses were synthesized in $Pt_{90}Rh_{10}$ crucibles using the melt-quenching method with analytical reagent-grade raw materials (SiO_2, H_3BO_3, Na_2CO_3, and $CaCO_3$). The chemical compositions of the final glasses were determined using inductively coupled plasma and flame emission spectroscopy; the results are reported in Table I. The high-B_2O_3-containing samples ($x = 37$, 50, and 75) were kept in containers with desiccant.

TABLE I. Analyzed chemical compositions, initial fraction of tetrahedral to total boron (N_4), and glass transition temperature (T_g) of the investigated glasses. Compositions are analyzed using inductively coupled plasma and flame emission spectroscopy, N_4 determined using ^{11}B MAS NMR spectroscopy, and T_g determined using differential scanning calorimetry at a rate of 10 K/ min. The errors in N_4 and T_g are ±2.5 at. % and ±2–3 K, respectively.

	Chemical composition (mol %)					
Glass ID	SiO_2	B_2O_3	CaO	Na_2O	N_4 (at. %)	T_g(K)
SLS	75.6	⋯	10.0	14.4	⋯	831
B15	58.4	16.5	10.1	15.0	70.0	843
B37[a]	36.9	38.4	10.6	14.1	53.5	813
B50[a]	24.9	49.3	10.8	15.0	48.9	803
B75[a]	⋯	74.1	10.5	15.4	39.9	775

[a] Data from Ref. [23].

Prior to compression, the glasses were annealed for ∼2 h at their respective T_g values to ensure uniform thermal history. T_g is determined using differential scanning calorimetry at 10 K/ min (Table I). Glass samples with dimensions of about $12 \times 12 \times 3$ mm^3 were then cut and the flats were optically polished. These samples were isostatically compressed by loading individual samples into a vertically positioned gas pressure chamber with an internal diameter of 6 cm. As described in detail elsewhere [24], a multizone cylindrical graphite furnace is placed inside the gas pressure reactor with nitrogen as the compression medium. The samples were heated at a constant rate of 600 K/h to their respective ambient pressure T_g values for each composition. The system is kept at these conditions under high nitrogen pressure (0.2, 0.4, 0.6, or 1.0 GPa) for 30 min. Afterwards the furnace is cooled down to room temperature at a constant rate of 60 K/min and the system is decompressed with a rate of 30 MPa/min at room temperature. X-ray-diffraction analyses of these samples showed no evidence of crystallization due to the treatment. We note that the glass transition temperature is a function of pressure [25], but the obtained data are all for a constant applied pressure and the value of viscosity at the compression temperature is thus approximately a fixed value for the comparisons made. Moreover, we make no assumptions about T_g as a function of pressure in our analyses and have simply picked a common temperature for the compression experiments.

Following compression, the samples are subjected to different types of characterization. Density (ρ) is determined using the Archimedes principle with water or ethanol as the immersion medium. Each measurement of sample weight is repeated at least ten times. Vickers microindentation (Duramin 5, Struers A/S) is used to study the micromechanical properties in air at room temperature using a dwell time of 15 s. Crack resistance is determined by performing indentations at different loads of 0.098, 0.25, 0.49, 0.98, 1.96, 2.94, 4.91, 9.81, and 19.6 N. Thirty indentations are performed at each load. The number of radial corner cracks is then counted. The crack resistance of the glasses is quantified as the load resulting in an average of two out of four radial cracks at the corner of the indentations [26]. Vickers hardness (H_V) and the crack-to-indent size ratio (c/a) are measured at a load of 9.81 N, where c is the indentation crack length (distance from indent center to crack tip) and a is the indent's half diagonal. The average values of H_V and c/a from thirty indents are reported.

^{11}B and ^{23}Na magic-angle-spinning (MAS) NMR experiments on the borosilicate glass with $x = 15$ (as-prepared and compressed at 1 GPa) are conducted at 16.4 T using a commercial spectrometer (VNMRS, Agilent) and MAS NMR probes. Resonance frequencies for ^{11}B and ^{23}Na at this external magnetic field strength are 224.51 and 185.10 MHz, respectively. Samples are crushed using an agate mortar and pestle, packed into 3.2-mm zirconia rotors and spun at frequencies of nominally 20 kHz. ^{11}B and ^{23}Na MAS NMR spectra are collected using short radio-frequency pulses (0.6 μs, equivalent to $\pi/12$ tip angles), relaxation delays of 5 s and signal averaging of 1000 to 2000 acquisitions. Data are frequency referenced to aqueous boric acid at 19.6 ppm and aqueous NaCl at 0 ppm for ^{11}B and ^{23}Na, respectively. ^{11}B MAS NMR spectra are fit using DMFIT [27] to reproduce B^{III} and B^{IV} line shapes, and N_4 values are determined from the integration of these resonances. N_4 values for the three as-prepared glasses with $x = 37$, 50, and 75 are taken from the previous study [23].

The soda-lime silicate glass ($x = 0$) compressed at 1 GPa is also subjected to isothermal annealing (relaxation) experiments at ambient pressure. The glass is annealed at 765 K (corresponding to $0.92T_g$, where T_g is the value prior to compression) by placing it in a preheated electric furnace. After the predetermined annealing time, the samples are rapidly quenched from the heated furnace. Density and hardness of the sample are then determined *ex situ* and the same sample is further annealed at the same temperature. The reported annealing time (between 2 and 5000 min) thus represents the sum of all the annealing intervals.

III. RESULTS

Figure 1(a) shows ^{11}B MAS NMR spectra of the as-prepared and compressed (at 1 GPa) borosilicate glass with $x = 15$. These spectra are characterized by a broad peak centered around +15 ppm, corresponding to trigonal boron (B^{III}) sites, and a relatively narrow peak centered around 0 ppm, corresponding to tetrahedral boron (B^{IV}) sites. The fraction of tetrahedral to total boron (N_4) is found through simulation of the spectral line shapes and subsequent integration. The values of N_4 for the glasses prior to compression are reported in Table I. The ^{11}B MAS NMR spectra and the quantification of N_4 for the three glasses with $x = 37$, 50, and 75 prior to compression have already been reported in Ref. [23]. We note that these previously published values of N_4 are uncorrected for overlapping satellite transition from the B^{IV} sites. To maintain consistency with these values, we also here report the uncorrected values of N_4, but note that our fits and analyses show that they are around ~2 at. % too high compared to the corrected values.

It is seen from Table I that N_4 increases with an increasing SiO_2/B_2O_3 ratio for the as-prepared glasses, as it has been previously found [28]. For the glass with $x = 15$, isostatic compression at T_g and 1 GPa causes an increase of N_4 from 70 to 77 at. %. For the glass with $x = 75$, we have previously found that N_4 increases from 39.9 to 41.1 at. % following isostatic compression at T_g and 0.57 GPa [17]. These changes in boron speciation due to pressurization are comparable with literature results for similar pressurization conditions [18].

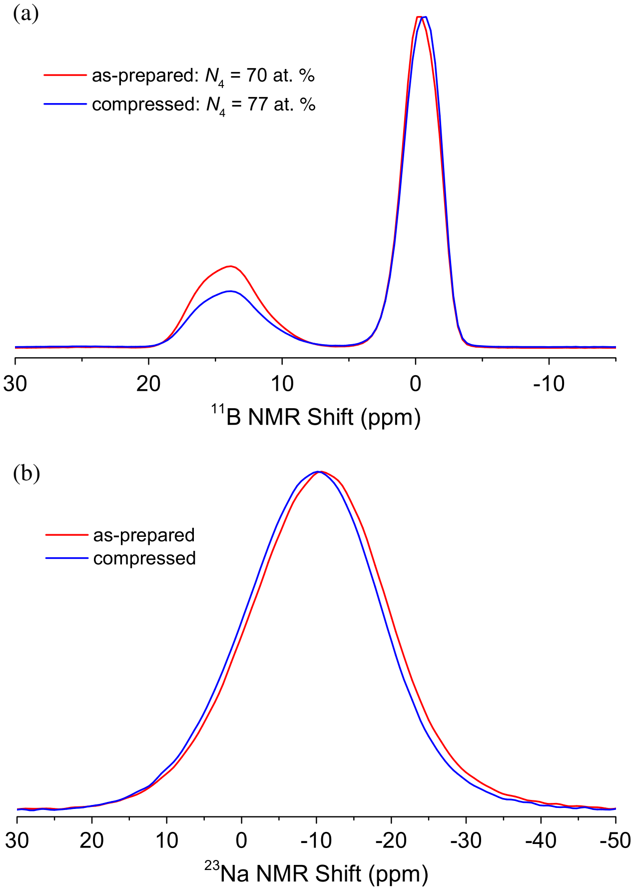

FIG. 1. (a) ^{11}B MAS and (b) ^{23}Na MAS NMR spectra at 16.4 T of the as-prepared and compressed (at 1 GPa) borosilicate glass with $x = 15$. The uncertainty of N_4 is ±2.5 at. %.

^{23}Na MAS NMR spectra show an increase in the frequency shift upon compression for the glass with $x = 15$ [Fig. 1(b)]. ^{23}Na 3QMAS NMR studies have also been conducted on the as-made and compressed B15 glasses, providing a means to determine if these changes to the MAS NMR line shape are due to isotropic chemical shift (δ_{iso}) or quadrupolar coupling product (P_Q). Evaluation of the 3QMAS NMR data, using the center of gravity in both the MAS and isotropic shift dimension, indicates that compression leads to a change in δ_{iso} only, with P_Q relatively unchanged (2.08 vs 2.03 MHz) in the B15 glass. This behavior is consistent with a shortening of Na—O bond length with pressure, and likely without any change in sodium coordination number [15,29,30], which is also consistent with other studies of sodium in glasses compressed at much higher pressures [31].

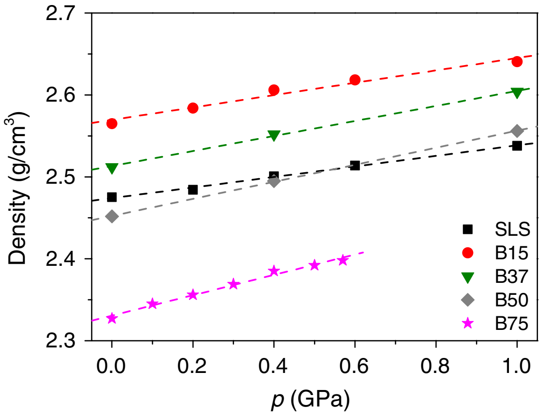

FIG. 2. Density of the five investigated glasses as a function of the applied isostatic pressure (p) at T_g. Errors associated with the density results are smaller than the size of the symbols. The dashed lines represent linear fits to the data ($R^2 \geq 0.97$). Data for the B75 glass are from Ref. [17].

The pressure dependence of density is shown in Fig. 2. Densification of the five glasses exhibits a linear dependence on pressure in the investigated pressure region, as previously found for other oxide glasses [13]. Likewise, Vickers hardness increases linearly with the applied isostatic pressure (Fig. 3), i.e., as the network densifies, a higher load is required to cause a given indent size. The rates of change in both density ($d\rho/dp$) and hardness (dH_V/dp) with pressure exhibit a composition dependence that will be discussed later.

The effect of pressurization on cracking behavior is displayed in Figs. 4 and 5. Figure 4(a) shows the percentage of radial cracks initiated by the sharp Vickers diamond for the SLS glass with different isostatic pressures. Similar crack-initiation-probability curves are collected for the other glasses. An increase in crack-initiation probability as a function of applied indentation load and isostatic pressure is seen for all glasses, in agreement with previous findings for other glasses [17]. The indentation load at which the crack-initiation probability would be 50% is

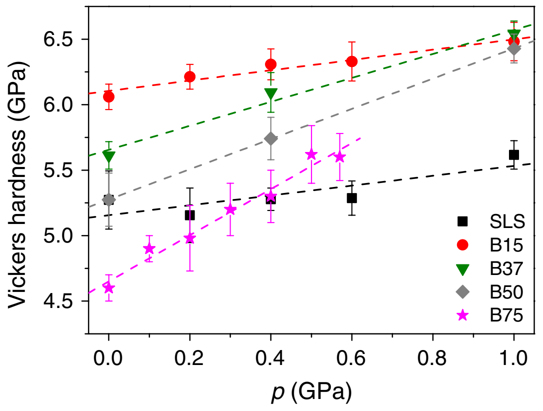

FIG. 3. Vickers hardness of the five investigated glasses as a function of the applied isostatic pressure (p) at T_g. Hardness is reported for an applied indentation load and dwell time of 9.81 N and 15 s, respectively. The dashed lines represent linear fits to the data ($R^2 \geq 0.70$). Data for the B75 glass are from Ref. [17].

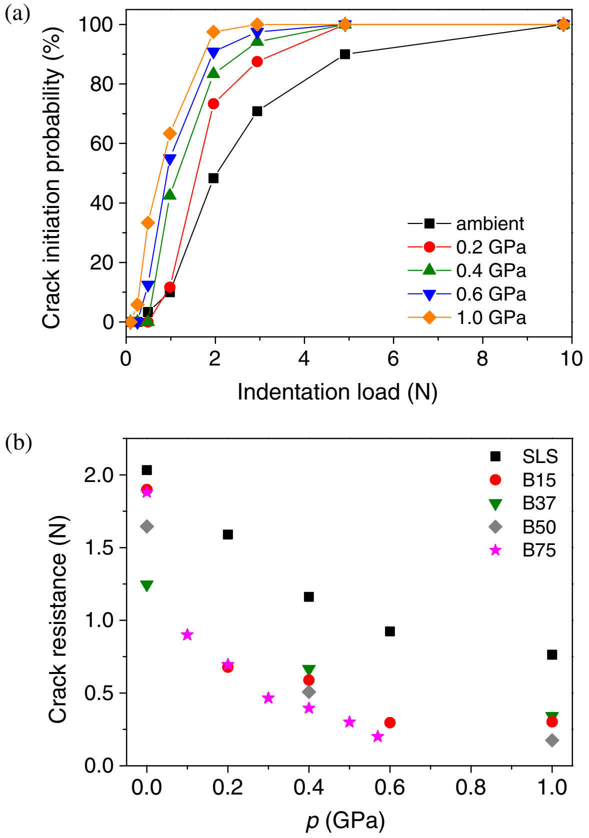

FIG. 4. (a) Crack-initiation probability as a function of the applied indentation load for the silicate (SLS) glass compressed at different isostatic pressures. (b) Pressure dependence of the crack resistance, which is calculated as the load that causes the crack-initiation probability to reach 50%. Data for the B75 glass are from Ref. [17].

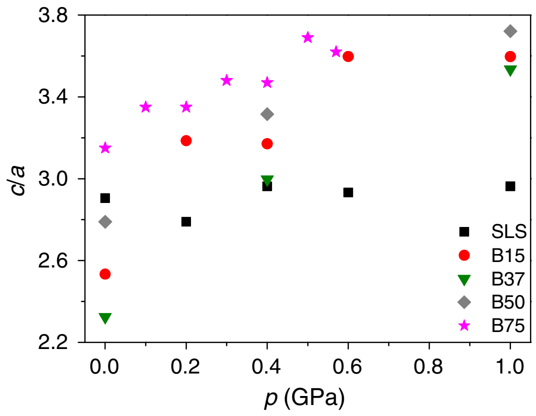

FIG. 5. Ratio of crack length to half diagonal of the indent (c/a) for applied indentation load of 9.81 N as a function of the isostatic pressure (p) of the five glasses. Data for the B75 glass are from Ref. [17].

referred to as the crack resistance, and its composition and pressure dependence is shown in Fig. 4(b). An overall decrease in crack resistance with increasing pressure is seen for the five glasses. Figure 5 shows the ratio of crack length to half diagonal of the indent (c/a) as a function of isostatic pressure for the five glasses. c and a are determined shortly (<20 s) after indentation ($P = 9.81$ N) to minimize subcritical crack growth. c/a generally increases with increasing isostatic pressure, which is indicative of increased brittleness [32].

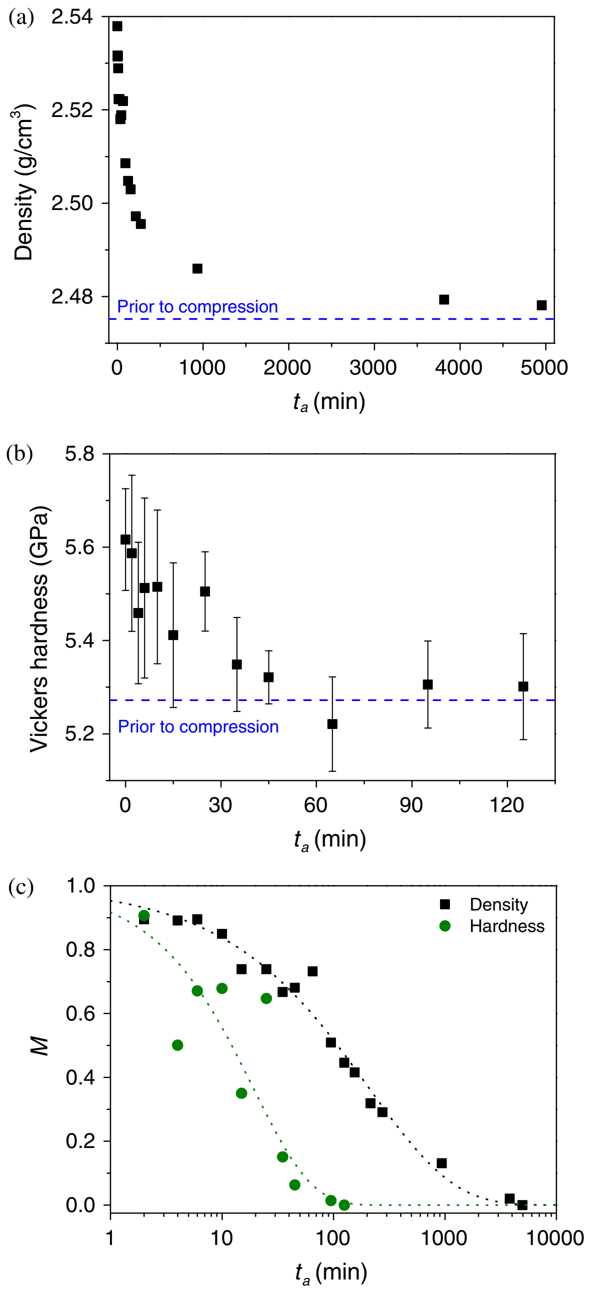

FIG. 6. Relaxation of density and hardness of the silicate (SLS) glass compressed at 1 GPa. Dependence of (a) density and (b) hardness on annealing time (t_a) at $0.92T_g$ (765 K) under ambient pressure. (c) Annealing time dependence of the relaxation function (M) for density and hardness. M is defined in Eq. (1). The dotted lines represent fits to Eq. (2).

The SLS glass isostatically compressed at 1 GPa is annealed under ambient pressure at $0.92T_g$ (765 K) for various durations (t_a). This annealing causes a decrease of density [Fig. 6(a)] and hardness [Fig. 6(b)] with increasing annealing duration, i.e., these properties of the compressed glass are relaxing towards those of the glass prior to compression. To describe the relaxation process of density and hardness of the compressed glass quantitatively, a relaxation function (M) is defined as the fraction of the property (P) unrelaxed at time t_a,

$$M(t_a) = \frac{P(t_a) - P(\infty)}{P(0) - P(\infty)} \tag{1}$$

$M(t_a)$ is then described by the Kohlrausch stretched exponential relaxation function [33],

$$M(t_a) = \exp\left[-\left(\frac{t_a}{\tau}\right)^{\beta}\right], \tag{2}$$

where τ is the characteristic relaxation time for the decay and $0 < \beta \leq 1$ is the dimensionless stretching exponent. The relaxation function decays from an initial value of $M(0) = 1$ to $M(\infty) = 0$ in the limit of infinite time. The upper limit of $\beta = 1$ corresponds to simple exponential decay, while lower values of β are indicative of a more complicated nonexponential relaxation process [34]. The fitted and experimental values of $M(t_a)$ are shown in Fig. 6(c) for relaxation of both density and hardness. Because of the relatively large error range and small changes in absolute values of the hardness data, no detailed discussion can be done based on the values of τ and β for hardness. However, it is clear that the relaxation time for hardness is significantly lower than that for density. For density relaxation, the fitted value of β is equal to 0.57, which is close to the Phillips value of 3/5 [34], in agreement with previous findings [16,24].

IV. DISCUSSION

To compare the extent of the density increase due to compression in the different glass compositions, we calculate the irreversible plastic compressibility, defined as $-(1/V)(dV/dp)$. This is the volume change measured after decompression to ambient pressure, i.e., the real compressibility would also contain an elastic (reversible) contribution, which we do not measure. Figure 7 illustrates the dependence of plastic compressibility on the concentration of B$^{\text{III}}$ units in the as-prepared glasses. Plastic compressibility is calculated from the slopes of the linear fits to density vs pressure in Fig. 2, whereas the concentration of trigonal boron is calculated based on the analyzed compositions and N_4 values from ^{11}B MAS NMR measurements in Fig. 1(a) and Ref. [23]. We note that the

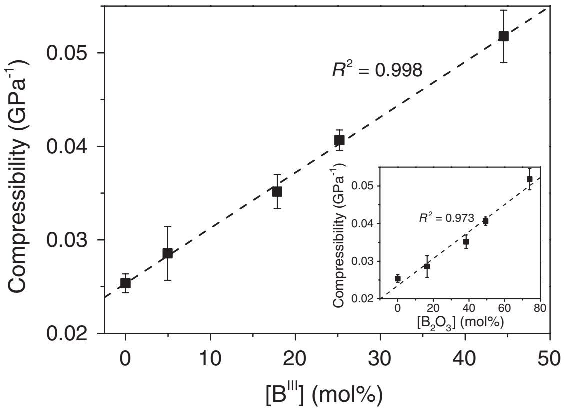

FIG. 7. Plastic (irreversible) compressibility plotted as a function of the concentration of trigonal boron units in the silicate (SLS), borate (B75), and three borosilicate (B15, B37, B50) glasses. Plastic compressibility is calculated from the slopes of the linear fits to density vs pressure in Fig. 2, whereas the concentration of trigonal boron is calculated based on the analyzed compositions and N_4 values from ^{11}B MAS NMR measurements. Inset: plastic compressibility as a function of the total concentration of B_2O_3. The dashed lines represent linear fits to the data.

concentration of trigonal boron plotted in Fig. 7 is that at ambient pressure prior to isostatic compression, since this value represents the number of species most disposed for structural modification during compression. The linear correlation between plastic compressibility and [B^{III}] has $R^2 = 0.998$, which is thus a stronger correlation than that between plastic compressibility and total B_2O_3 content with $R^2 = 0.973$ (inset of Fig. 7). To the best of our knowledge, no detailed studies on the structural changes of borate glasses at ≤ 1 GPa and T_g have been conducted, but the main densification mechanism of these glasses at higher pressures has been suggested to consist of changes in the ring structures of the borate network [35–38]. The boron units disposed toward densification are therefore best represented by the amount of trigonal boron present in the as-prepared glass. These are also the boron units which are susceptible for coordination number change upon compression. Establishing the correlations among plastic compressibility and different structural units may be helpful in the design of new damage-resistant glass compositions [22,39], as the pressure-induced deformations during mechanical load lead to structural and topological rearrangements that are important to understand for clarifying fracture origins.

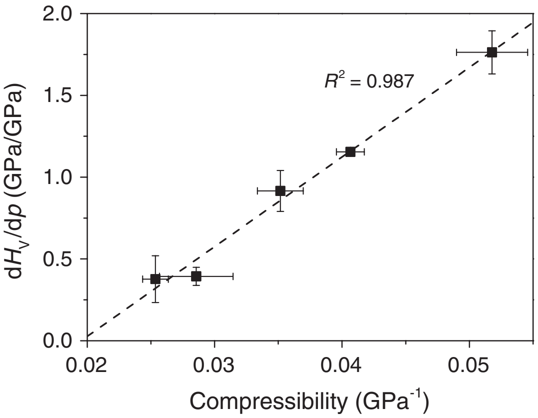

FIG. 8. Dependence of the slopes of the curves (dH_V/dp) in Fig. 3 on the plastic compressibility for the silicate (SLS), borate (B75), and three borosilicate (B15, B37, B50) glasses. Plastic compressibility is calculated from the slopes of the linear fits to density vs pressure in Fig. 2.

Both density (Fig. 2) and hardness (Fig. 3) correlate linearly with the applied isostatic pressure, in agreement with previous findings [17,18]. In addition, a linear correlation between the slope of the hardness vs pressure (dH_V/dp) and plastic compressibility can be seen (Fig. 8), suggesting that the overall network densification is responsible for the increase in hardness upon compression. This correlation during mechanical densification does not apply, however, during subsequent thermal relaxation (annealing). Here a decoupling between hardness and density relaxation is found for the compressed SLS glass [Fig. 6(c)] and previously also for a borate glass [18]. Changes in glass properties with densification have previously been found to exhibit different dependences on density, depending on whether densification is achieved by thermal or mechanical treatment [40]. This result indicates that identical densities, achieved either by thermal or mechanical treatment, may not necessarily result in identical glass structures. However, the fact that the density and hardness values of the thermally relaxed glass approach those of the as-prepared glass suggests the existence of structural similarities between the two. Previously, thermal relaxation of a mechanically densified sodium borosilicate glass has been suggested to be viscosity driven [16], with intermediate-range recovery governing macroscopic density relaxation [41]. That is, intermediate-range structures may be similar in the thermally relaxed and the as-prepared glasses. During thermal relaxation of a compressed borate glass at $0.9T_g$, the tetrahedral boron fraction and sodium environments (i.e., short-range ordering) have, however, been found to remain constant during thermal density relaxation [18], viz., the relaxed and as-prepared glasses have different glass structures, despite having similar density. Unfortunately, these findings do not allow for an identification of the structural origins of the decoupling between density and hardness during thermal relaxation [Fig. 6(c)], since intermediate-range ordering is found to be correlated with density, whereas short-range ordering is expected to remain constant during hardness and density relaxation at $0.92T_g$ [18]. However, the finding that density changes can occur without a corresponding hardness change [see longest annealing times in Fig. 6(c)] is a surprising result, and the potential isolation of key structural features governing macroscopic properties may be possible by further structural studies of these types of density modifications.

The mechanical properties (hardness, crack resistance, and brittleness) exhibit different dependences on composition and pressure [Figs. 9(a)–9(c)]. Hardness and c/a both increase following compression for all glass compositions, but they display extrema at different SiO_2/B_2O_3 ratios. For all the as-prepared samples, crack resistance and c/a both exhibit minimum values for the composition with approximately equal concentrations of SiO_2 and B_2O_3, but the compositional trends of these properties are significantly changed following compression. Furthermore, it should be noted that the SLS glass only exhibits minor changes in hardness and c/a but large change in crack resistance upon compression. These differences in the composition and pressure dependence of the mechanical properties suggest they have different structural origins. Hence, the hot isostatic compression method offers a way to balance different mechanical properties when varying composition and pressure, which may have important practical implications. For example, the introduction of small amounts of B_2O_3 in the silicate end-member glass significantly increases hardness at ambient pressure, which is further increased upon compression (Fig. 3). However, the introduction of B_2O_3 also causes an increase of brittleness upon compression, which is avoided in the silicate end-member glass (Fig. 5).

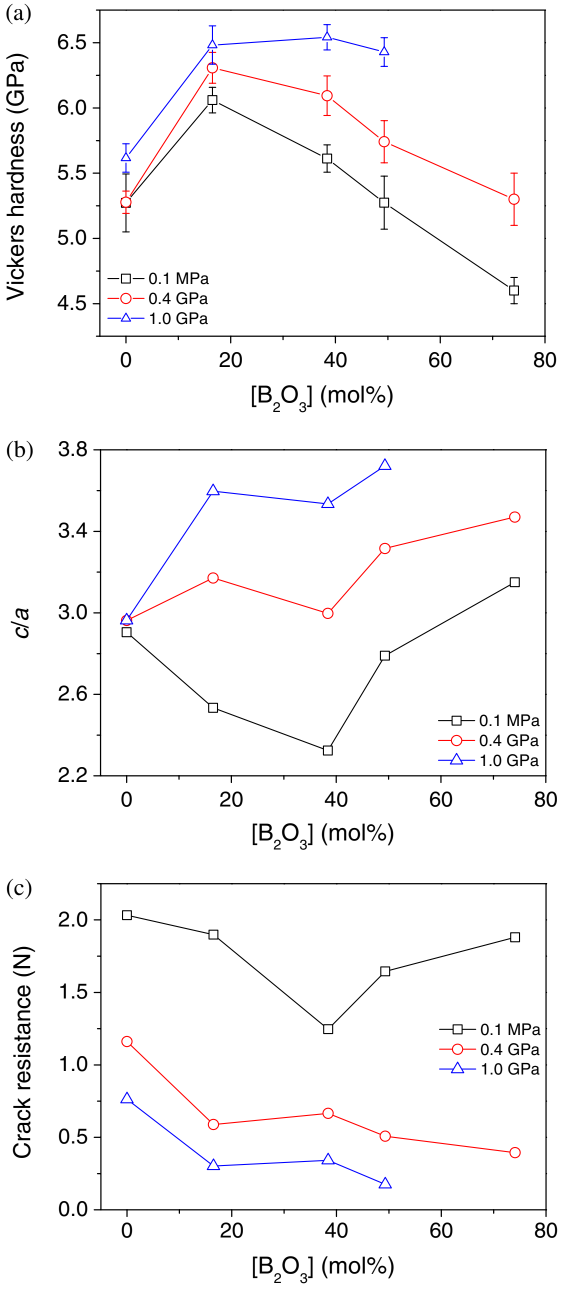

FIG. 9. Dependence of the mechanical properties on composition and pressure (0.1 MPa, 0.4 GPa, and 1.0 GPa). (a) Vickers hardness from Fig. 3. (b) Ratio of crack length to half diagonal of the indent (c/a) from Fig. 5. (c) Crack resistance from Fig. 4(b).

The compositional dependence of Vickers hardness of soda-lime borate [42] and soda-lime borosilicate [23] glasses has previously been successfully predicted using temperature-dependent constraint theory. According to this model [42], hardness is proportional to the number of network constraints in excess of 2.5, with an unknown proportionality constant (dH_V/dn):

$$H_V(x) = \left(\frac{dH_V}{dn}\right)[n(x) - 2.5], \tag{3}$$

where $n(x)$ is the number of room-temperature constraints (two-body bond length and three-body bond angular) for the composition x. The pressure treatment will change the number of constraints due to network-former coordination number changes. Hence, an increase in n is only expected to be the result of an increasing fraction of tetrahedral boron (viz., B^{IV} contributes more constraints than B^{III}). By using the ^{11}B MAS NMR data from Fig. 1(a), the calculated increase in hardness due to the change in boron speciation for the B15 glass is a maximum of 0.2 GPa [23]. This increase is less than half of the observed value (Fig. 3). Furthermore, the change in boron coordination number has previously been found to be decoupled from the pressure-induced change in hardness [18]. These results indicate that the network densification also changes the scaling factor (dH_V/dn) in the model of Eq. (3), i.e., there is a larger increase in hardness per constraint for a densified than as-prepared glass structure.

The pressure-induced structural changes suggested to occur in borate and silicate glasses within the pressure regime below 5 GPa include changes in the silica and borate ring networks [15,43,44], an increase in the number of silicon first neighbors surrounding tetrahedral boron [45] (with the “tetrahedral boron avoidance” principle as a good approximation in pressurized borosilicate glasses [45]), a reduction in the number of nonbridging oxygen on silica tetrahedra accompanying the conversion of B^{III} to B^{IV} [45], and a compression of Na-O bond lengths [15,18]. These topological changes may affect the rigidity of the network constraints and accordingly affect the mechanical properties. However, the same topological description used to describe the composition dependence of hardness cannot be applied to the other mechanical properties (brittleness and crack resistance), since they follow other compositional and pressure dependencies (Fig. 9).

V. CONCLUSIONS

Isostatic pressure-induced changes in density and micromechanical properties of soda-lime borosilicate glasses exhibit pronounced composition dependence. Plastic compressibility is found to be strongly correlated with the B_2O_3 content, particularly with the content of trigonal boron units present in the as-prepared glass. This dependence may arise because the trigonal boron units are the structural elements most prone to densification during compression. A linear correlation between pressure-induced hardness and density changes is also found. On the other hand, these properties are found to be decoupled during subsequent thermal relaxation at ambient pressure, which may be because thermal and mechanical structural modifications operate through different mechanisms. Finally, the micromechanical analyses show that hardness, crack resistance, and brittleness exhibit significantly different pressure and composition dependences, indicating their different structural origins. The presented hot isostatic compression method thus offers wide versatility in terms of tailoring a combination of glass properties that are suitable for a particular composition or application based on the intended function. Understanding the response of glasses to high pressure is also important for clarifying fracture origins during mechanical load, as the pressure-induced deformations lead to structural and topological rearrangements. Establishing correlations between plastic compressibility and different structural units may thus be helpful in the design of new damage-resistant glass compositions.

ACKNOWLEDGMENTS

M. N. S. and M. M. S. acknowledge the support from the Danish Council for Independent Research under Sapere Aude: DFF-Starting Grant (No. 1335-00051A). S. J. R. acknowledges the support from the National Science Center of Poland under Grant No. UMO-2011/03/B/ST3/02352.

T. K. B., S. D. F., R. H. P., A. Ø. T., and M. B. Ø. contributed equally to this work.

[1] K. Chang, M. M. Dacorogna, M. L. Cohen, J. Mignot, G. Chouteau, and G. Martinez, Superconductivity in high-pressure metallic phases of Si, Phys. Rev. Lett. **54**, 2375 (1985).
[2] G. H. Wolf and P. F. McMillan, *Pressure effects on silicate melt—Structure and properties*, in Review in Mineralogy Vol. 32, edited by J. F. Stebbins, D. Dingwell, and P. F. McMillan (Mineralogical Society of America, Washington, DC, 1995), pp. 505–561.
[3] P. F. McMillan, Polyamorphic transformations in liquids and glasses, J. Mater. Chem. **14**, 1506 (2004).
[4] P. F. McMillan, M. Wilson, M. C. Wilding, D. Daisenberger, M. Mezouar, and G. N. Greaves, Polyamorphism and liquid-liquid phase transitions: Challenges for experiment and theory, J. Phys. Condens. Matter **19**, 415101 (2007).
[5] O. Mishima, L. D. Calvert, and E. Whalley, An apparently first-order transition between two amorphous phases of ice induced by pressure, Nature (London) **314**, 76 (1985).
[6] T. Morishita, High density amorphous form and polyamorphic transformations of silicon, Phys. Rev. Lett. **93**, 055503 (2004).
[7] S. Sen, S. Gaudio, B. G. Aitken, and C. E. Lesher, Observation of a pressure-induced first-order polyamorphic transition in a chalcogenide glass at ambient temperature, Phys. Rev. Lett. **97**, 025504 (2006).
[8] H. W. Sheng, H. Z. Liu, Y. Q. Cheng, J. Wen, P. L. Lee, W. K. Luo, S. D. Shastri, and E. Ma, Polyamorphism in a metallic glass, Nat. Mater. **6**, 192 (2007).
[9] J. C. Mauro, C. S. Philip, D. J. Vaughn, and M. S. Pambianchi, Glass science in the United States: Current status and future directions, Int. J. Appl. Glass Sci. **5**, 2 (2014).
[10] S. K. Lee, Probing of bonding changes in B_2O_3 glasses at high pressure with inelastic x-ray scattering, Nat. Mater. **4**, 851 (2005).
[11] R. J. Hemley, H. K. Mao, P. M. Bell, and B. O. Mysen, Raman Spectroscopy of SiO_2 glass at high pressure, Phys. Rev. Lett. **57**, 747 (1986).
[12] J. E. Dickinson, C. M. Scarfe, and P. McMillan, Physical properties and structure of $K_2Si_4O_9$ melt quenched from pressures up to 2.4 GPa, J. Geophys. Res. **95**, 15675 (1990).
[13] L. Wondraczek, S. Sen, H. Behrens, and R. E. Youngman, Structure-energy map of alkali borosilicate glasses: Effects of pressure and temperature, Phys. Rev. B **76**, 014202 (2007).
[14] L. Wondraczek, H. Behrens, Y. Z. Yue, J. Deubener, and G. W. Scherer, Relaxation and glass transition in an isostatically compressed diopside glass, J. Am. Ceram. Soc. **90**, 1556 (2007).
[15] J. S. Wu, J. Deubener, J. F. Stebbins, L. Grygarova, H. Behrens, L. Wondraczek, and Y. Z. Yue, Structural response of a highly viscous aluminoborosilicate melt to isotropic and anisotropic compressions, J. Chem. Phys. **131**, 104504 (2009).
[16] L. Wondraczek, S. Krolikowski, and H. Behrens, Kinetics of pressure relaxation in a compressed alkali borosilicate glass, J. Non-Cryst. Solids **356**, 1859 (2010).
[17] S. Striepe, M. M. Smedskjaer, J. Deubener, U. Bauer, H. Behrens, M. Potuzak, R. E. Youngman, J. C. Mauro, and Y. Z. Yue, Elastic and micromechanical properties of isostatically compressed soda–lime–borate glasses, J. Non-Cryst. Solids **364**, 44 (2013).
[18] M. M. Smedskjaer, R. E. Youngman, S. Striepe, M. Potuzak, U. Bauer, J. Deubener, H. Behrens, J. C. Mauro, and Y. Z. Yue, Irreversibility of pressure induced boron speciation change in glass, Sci. Rep. **4**, 3770 (2014).

[19] L. Wondraczek, J. C. Mauro, J. Eckert, U. Kühn, J. Horbach, J. Deubener, and T. Rouxel, Towards ultrastrong glasses, Adv. Mater. **23**, 4578 (2011).

[20] P. Sellapan, T. Rouxel, F. Celarie, E. Becker, P. Houizot, and R. Conradt, Composition dependence of indentation deformation and indentation cracking in glass, Acta Mater. **61**, 5949 (2013).

[21] T. Rouxel, P. Sellapan, F. Celarie, and P. Houizot, Toward glasses with better indentation cracking resistance, C. R. Mec. **342**, 46 (2014).

[22] M. J. Dejneka, A. J. Ellison, and J. C. Mauro, Zircon compatible, ion exchangeable glass with high damage resistance, U.S. Patent Application PCT/US2013/042840 (2013).

[23] M. M. Smedskjaer, J. C. Mauro, R. E. Youngman, C. L. Hogue, M. Potuzak, and Y. Z. Yue, Topological principles of borosilicate glass chemistry, J. Phys. Chem. B **115**, 12930 (2011).

[24] M. M. Smedskjaer, S. J. Rzoska, M. Bockowski, and J. C. Mauro, Mixed alkaline earth effect in the compressibility of aluminosilicate glasses, J. Chem. Phys. **140**, 054511 (2014).

[25] A. Drozd-Rzoska, S. J. Rzoska, M. Paluch, A. R. Imre, and C. M. Roland, On the glass transition temperature under extreme pressures, J. Chem. Phys. **126**, 164504 (2007).

[26] M. Wada, H. Furukawa, and K. Fujita, Crack resistance of glasses on Knoop scratch test, in *Proceedings of 10th International Congress on Glass* (Ceramic Society of Japan, Tokyo, 1974), Vol. 11, p. 39.

[27] D. Massiot, F. Fayon, M. Capron, I. King, S. Le Calve, B. Alonso, J. O. Durand, B. Bujoli, Z. Gan, and G. Hoatson, Modelling one- and two-dimensional solid-state NMR spectra, Magn. Reson. Chem. **40**, 70 (2002).

[28] S. K. Lee and J. F. Stebbins, Extent of intermixing among framework units in silicate glasses and melts, Geochim. Cosmochim. Acta **66**, 303 (2002).

[29] S. K. Lee and J. F. Stebbins, The distribution of sodium ions in aluminosilicate glasses: A high field Na-23 MAS and 3Q MAS NMR study, Geochim. Cosmochim. Acta **67**, 1699 (2003).

[30] A. M. George and J. F. Stebbins, Dynamics of Na in sodium aluminosilicate glasses and liquids, Phys. Chem. Miner. **23**, 526 (1996).

[31] S. K. Lee, Effect of pressure on structure of oxide glasses at high pressure: Insights from solid-state NMR of quadrupolar nuclides, Solid State Nucl. Magn. Reson. **38**, 45 (2010).

[32] J. Sehgal and S. Ito, A new low-brittleness glass in the soda-lime-silica glass family, J. Am. Ceram. Soc. **81**, 2485 (1998).

[33] R. Kohlrausch, Theorie des elektrischen Rückstandes in der Leidener flasche, Ann. Phys. (Berlin) **167**, 179 (1854).

[34] J. C. Phillips, Stretched exponential relaxation in molecular and electronic glasses, Rep. Prog. Phys. **59**, 1133 (1996).

[35] M. Grimsditch, A. Polian, and A. C. Wright, Irreversible structural changes in vitreous B_2O_3 under pressure, Phys. Rev. B **54**, 152 (1996).

[36] V. V. Brazhkin, I. Farnan, K. Funakoshi, M. Kanzaki, Y. Katayama, A. G. Lyapin, and H. Saitoh, Structural transformations and anomalous viscosity in the B_2O_3 melt under high pressure, Phys. Rev. Lett. **105**, 115701 (2010).

[37] G. Carini Jr., E. Gilioli, G. Tripodo, and C. Vasi, Structural changes and elastic characteristics of permanently densified vitreous B_2O_3, Phys. Rev. B **84**, 024207 (2011).

[38] S. K. Lee, P. J. Eng, and H.-K. Mao, Probing and modeling of pressure-induced coordination transformation in borate glasses: Inelastic x-ray scattering study at high pressure, Phys. Rev. B **78**, 214203 (2008).

[39] J. C. Mauro, A. J. Ellison, and L. D. Pye, Glass: The nanotechnology connection, Int. J. Appl. Glass Sci. **4**, 64 (2013).

[40] R. J. Charles, Structural state and diffusion in a silicate glass, J. Am. Ceram. Soc. **45**, 105 (1962).

[41] S. Riebstein, L Wondraczek, D. de Ligny, S. Krolikowski, S Sirotkin, J. P. Simon, V. Martinez, and B. Champagnon, Structural heterogeneity and pressure-relaxation in compressed borosilicate glasses by *in situ* small angle x-ray scattering, J. Chem. Phys. **134**, 204502 (2011).

[42] M. M. Smedskjaer, J. C. Mauro, and Y. Z. Yue, Prediction of glass hardness using temperature-dependent constraint theory, Phys. Rev. Lett. **105**, 115503 (2010).

[43] T. Deschamps, C. Martinet, D. de Ligny, and B. Champagnon, Elastic anomalous behavior of silica glass under high-pressure: *In-situ* Raman study, J. Non-Cryst. Solids **355**, 1095 (2009).

[44] Z. Zhang and N. Soga, Structural study of densified borate glasses by Raman and infrared spectroscopy, Phys. Chem. Glasses **32**, 142 (1991).

[45] L. S. Du, J. R. Allwardt, B. C. Schmidt, and J. F. Stebbins, Pressure-induced structural changes in a borosilicate glass-forming liquid: Boron coordination, non-bridging oxygens, and network ordering, J. Non-Cryst. Solids **337**, 196 (2004).